

HIP-2009-01/TH  
 IPPP/09/01  
 DCPT/09/02  
 MAN/HEP/2009/4  
 NORDITA-2009-14

## Searching for the triplet Higgs sector via central exclusive production at the LHC

M. Chaichian<sup>1</sup>, P. Hoyer<sup>1</sup>, K. Huitu<sup>1</sup>, V.A. Khoze<sup>2,3</sup>, and A.D. Pilkington<sup>3</sup>

<sup>1</sup>*Department of Physics, University of Helsinki, and Helsinki Institute of Physics, P.O. Box 64, FIN-00014 University of Helsinki, Finland*

<sup>2</sup>*Institute for Particle Physics Phenomenology, University of Durham, Durham, DH1 3LE, UK*

<sup>3</sup>*School of Physics & Astronomy, University of Manchester, Manchester M13 9PL, UK*

### Abstract

We discuss the prospects of searching for the neutral Higgs bosons of the triplet model in central exclusive production at the LHC. A detailed Monte Carlo analysis is presented for six benchmark scenarios for the Higgs boson,  $H_1^0$ , these cover  $m_{H_1^0} = 120, 150$  GeV and doublet-triplet mixing of  $c_H = 0.2, 0.5$  or  $0.8$ . We find that, for appropriate values of  $c_H$ , an excellent Higgs mass measurement is possible for the neutral Higgs in the triplet model, and discuss how to distinguish the triplet model Higgs boson from the Higgs boson of the Standard Model.

## 1 Introduction

It is expected that the nature of electroweak symmetry breaking will be revealed by the LHC experiments in the near future. In the Standard Model (SM), the electroweak symmetry is spontaneously broken by a Higgs doublet, which contains a neutral scalar field that acquires a vacuum expectation value (VEV). However, several Higgs multiplets typically occur in extensions to the SM. In supersymmetric models, at least one additional doublet is required. In left-right symmetric models, triplets are added to naturally generate a small mass for the neutrinos. Although the new scalars do not always take part in the electroweak symmetry breaking, they affect the properties of the Higgs boson through mixing.

Models with an extended Higgs sector typically contain charged scalars. A large number of studies [1, 2] have previously investigated the possibility of studying the doubly or singly charged components of higher representation<sup>1</sup>.

<sup>1</sup>For example the discovery of the  $ZW^{(+)}H^{(-)}$  and/or  $W^-W^-H^{++}$  vertices would serve as a direct proof of the non-standard structure of the Higgs sector (see *e.g.* [3]).

However the charged scalars may be considerably heavier than the light neutral bosons. Therefore, it would be instructive to study the properties of the light neutral Higgs particles in order to reveal the manifestation of new representations [4].

Higgs triplets are an especially attractive possibility [5]. A tiny neutrino mass may indicate that the mass is being generated by the seesaw mechanism containing the coupling of neutrinos to the triplet. In addition, composite Higgs models contain several multiplets, including the triplet ones. Triplets also occur in the little Higgs models - see, for example, [6] and references therein.

Determining that a new detected state is indeed a Higgs boson and distinguishing it from the Higgs boson of the SM will be far from trivial. This task will require a comprehensive programme of precision Higgs measurements. In particular, it will be of utmost importance to determine the spin and  $CP$  properties of a new state and to measure precisely its mass, width and couplings. In this work, we suggest that the neutral sector of the triplet representation can be studied using the central exclusive production (CEP) mechanism (see, for example, [7]) if forward proton detectors are installed at ATLAS and/or CMS, (see [8]).

The structure of the paper is as follows. In Sec. 2, we consider the general properties of models with higher representations. We then concentrate on the triplet representation in Sec. 3; we choose a benchmark model with the electroweak  $\rho$ -parameter equal to unity at tree-level, although the results are quite general. In Sec. 4, we introduce the central exclusive production process. Finally, in Sec. 5, we present a detailed Monte Carlo analysis of the central exclusive production of a neutral Higgs boson in the triplet model for a selection of parameter choices.

## 2 Models with general Higgs representations

We start with the Standard Model gauge group  $SU(2)_L \times U(1)_Y$  for the electroweak sector. The masses of the gauge bosons are then obtained from the kinetic part of Lagrangian,

$$L_{kin} = \sum_k (D^\mu \phi_k)^* (D_\mu \phi_k) + \frac{1}{2} \sum_i (D^\mu \xi_i)^T (D_\mu \xi_i), \quad (1)$$

where  $\phi_k$  are complex representations and  $\xi_i$  are real ones. The covariant derivative is

$$D_\mu = \partial_\mu + igW_\mu^a T^a + \frac{Y}{2} g' B_\mu, \quad (2)$$

where  $T^a$  is the generator of  $SU(2)$  in the appropriate representation (with  $\text{Tr}(T^a T^b) = \frac{1}{2} \delta^{ab}$ ) and  $Y$  is the  $U(1)$  hypercharge. Here  $W^a$  and  $B$  are the

SU(2) and U(1) gauge bosons respectively, and the mixing angle  $\theta_W$  of the  $Z$  boson and photon is obtained by diagonalizing the neutral sector. The  $W$  and  $Z$  boson masses are given by

$$m_Z^2 = (g^2 + g'^2) \sum_i T_{3i}^2 v_i^2, \quad m_W^2 = g^2 \sum_i T_{3i}^2 v_i^2, \quad (3)$$

where  $T_{3i}$  is the isospin third component and  $v_i$  is the VEV of particle  $i$ . It is clear from Eq. (3) that the doublet VEV decreases when several representations obtain non-vanishing VEVs. Furthermore, since the left-handed fermions are in doublets, the charged fermions can only get their masses through the Higgs doublet representation<sup>2</sup>,  $m_f = y_f v_{doublet}$ , and the fermion Yukawa coupling,  $y_f$ , must increase to produce the fermion masses. This, for example, leads to an enhancement in the production cross section for Higgs production via gluon fusion, where the dominant contribution is due to the top quark loop. A further enhancement is present in the branching ratio to fermion anti-fermion pairs. The possibility arises, therefore, of observing a very different prediction to that of the Standard Model.

The higher Higgs representations are severely restricted by the electroweak  $\rho$ -parameter. The  $\rho$ -parameter in the Standard Model is defined by the ratio of the gauge boson masses,

$$\rho = \frac{m_W^2}{m_Z^2 \cos^2 \theta_W}, \quad (4)$$

which at tree level is exactly unity in the Standard Model. The radiative corrections to the  $\rho$ -parameter have been studied in the SM up to three-loop level [9] - [15]<sup>3</sup>. For  $m_H \sim 2m_W$ , the correction to the  $\rho$ -parameter is  $\rho - 1 \sim -0.00078 + (4\text{-loop and higher corrections})$ . For heavier Higgs masses, the absolute value of the negative corrections increase. In a model with several scalar representations, whose neutral component develops a VEV, the  $\rho$ -parameter is given at tree level by [18]

$$\rho = \frac{\sum_i r_i (T_i(T_i + 1) - T_{3i}^2) v_i^2}{\sum_i 2T_{3i}^2 v_i^2}. \quad (5)$$

Here  $T_i$  is the weak isospin and  $r_i = 1/2(1)$  for real (complex) representations (see Eq. (7) for examples). Finally, the  $\rho$ -parameter is experimentally constrained to be [19],

$$\rho - 1 = 0.0002 \begin{array}{l} +0.0024 \\ -0.0009 \end{array}, \quad (6)$$

---

<sup>2</sup>For the neutral fermions this is not the case, since the Majorana masses can be generated through triplets.

<sup>3</sup>An explicit formula for the one-loop correction  $\Delta\rho^{(1)}$  in  $\rho = \Delta\rho^{(1)} + \Delta\rho^{(2)} + \Delta\rho^{(3)}$  is given in [16], two-loop terms are given in [17], and three-loop corrections in [15].

where the quoted errors are at  $2\sigma$ . As the loop-corrections to the  $\rho$ -parameter in the SM are negative, it can be argued that the  $\rho$ -parameter favors either a light Higgs boson or models that result in positive corrections to  $\rho$ .

### 3 Higgs bosons in a triplet model

In order to fulfill the experimental constraint on the  $\rho$ -parameter in Eqn. (6), the triplet VEV has to be small. Using Eqs. (5) and (6) one finds that the upper limit for the triplet VEV is a few GeV's assuming that there is one triplet in addition to one doublet. An alternative method to satisfy the experimental constraint at tree-level<sup>4</sup> is to have representations which add up to  $\rho = 1$ . We discuss this next.

#### 3.1 A model with $\rho = 1$

We consider the model developed by Georgi and Machacek [1], and further studied in [21, 22, 23] in which additional representations are chosen in such a way that the tree-level value of  $\rho$  remains unity. The  $\rho$ -parameter is fixed to one by choosing one complex scalar doublet ( $\phi_{Y=1}$ ) and two triplets, one real ( $\xi_{Y=0}$ ) and one complex ( $\chi_{Y=2}$ ). These can be written as

$$\phi = \begin{pmatrix} \phi^{0*} & \phi^+ \\ \phi^- & \phi^0 \end{pmatrix}, \quad \chi = \begin{pmatrix} \chi^0 & \xi^+ & \chi^{++} \\ \chi^- & \xi^0 & \chi^+ \\ \chi^{--} & \xi^- & \chi^{0*} \end{pmatrix}. \quad (7)$$

The following sign conventions are chosen:  $\phi^- = -(\phi^+)^*$ ,  $\chi^{--} = (\chi^{++})^*$ ,  $\chi^- = -(\chi^+)^*$ ,  $\xi^- = -(\xi^+)^*$ , and  $\xi^0 = (\xi^0)^*$ . The VEVs of the neutral components of the Higgs fields are denoted by  $\langle \chi^0 \rangle = \langle \xi^0 \rangle = b$  and  $\langle \phi^0 \rangle = a/\sqrt{2}$ . For doublet-triplet mixing, the standard notation is employed:

$$c_H \equiv \frac{a}{\sqrt{a^2 + 8b^2}}, \quad s_H \equiv \frac{\sqrt{8b}}{\sqrt{a^2 + 8b^2}}, \quad v^2 \equiv a^2 + 8b^2. \quad (8)$$

The most general scalar potential for the model, assuming invariance under  $\chi \rightarrow -\chi$ , is

$$\begin{aligned} V = & \lambda_1(\text{Tr}\phi^\dagger\phi - c_H^2 v^2)^2 + \lambda_2(\text{Tr}\chi^\dagger\chi - \frac{3}{8}s_H^2 v^2)^2 \\ & + \lambda_3(\text{Tr}\phi^\dagger\phi - c_H^2 v^2 + \text{Tr}\chi^\dagger\chi - \frac{3}{8}s_H^2 v^2)^2 \\ & - \lambda_4 \left( \text{Tr}\phi^\dagger\phi \text{Tr}\chi^\dagger\chi - 2 \sum_{ij} \text{Tr}(\phi^\dagger \tau_i \phi \tau_j) \text{Tr}(\chi^\dagger t_i \chi t_j) \right) \\ & + \lambda_5 \left( 3\text{Tr}(\chi^\dagger \chi \chi^\dagger \chi) - (\text{Tr}\chi^\dagger \chi)^2 \right), \end{aligned} \quad (9)$$

<sup>4</sup>At one-loop level, one has to consider renormalization. It has been shown in [20] that  $\rho \neq 1$  at tree-level is acceptable in a real triplet model as the experimental measurement of  $\rho$  is satisfied after calculating higher order corrections.

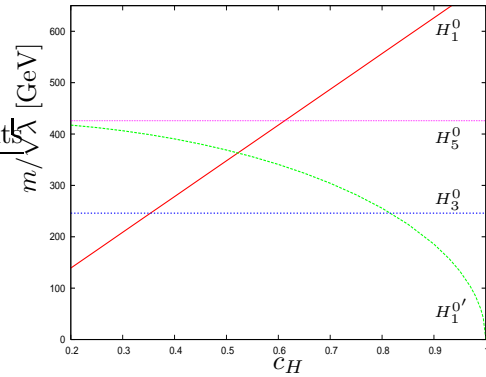


Figure 1: Masses of the Higgs bosons,  $m_{H_i}$ , divided by the unknown  $\sqrt{\lambda_i}$  couplings, as a function of  $c_H$ .

where  $\tau_i/2$  are the SU(2) generators in the doublet representation and  $t_i$  in the triplet representation.

As we are interested in this model mainly to illustrate the possibility of studying a neutral triplet Higgs sector, it is enough to limit ourselves to the case in which  $\lambda_3$  is zero and  $\lambda_4 = \lambda_5$ . The tree-level results of this triplet model are sufficient for demonstrating the phenomenology of the higher representations. In this case, the neutral doublet and triplet do not mix and the neutral mass eigenstates are

$$\begin{aligned} H_1^0 &= \phi^{0r}, & H_1^{0'} &= \frac{1}{\sqrt{3}}(\sqrt{2}\chi^{0r} + \xi^0), \\ H_3^0 &= c_H \chi^{0i} + s_H \phi^{0i}, & H_5^0 &= \frac{1}{\sqrt{3}}(\sqrt{2}\xi^0 - \chi^{0r}), \end{aligned} \quad (10)$$

where  $\chi^0 = (\chi^{0r} + i\chi^{0i})/\sqrt{2}$ . The masses of the neutral scalars are

$$\begin{aligned} m_{H_1^0}^2 &= 8c_H^2 \lambda_1 v^2, & m_{H_1^{0'}}^2 &= 3s_H^2 \lambda_2 v^2, \\ m_{H_3^0}^2 &= \lambda_4 v^2, & m_{H_5^0}^2 &= 3(\lambda_5 s_H^2 + \lambda_4 c_H^2) v^2. \end{aligned} \quad (11)$$

The lightest neutral scalar can be  $H_1^0$  if either  $c_H$  or  $\lambda_1$  is small - the  $m/\sqrt{\lambda_i}$  values are shown in Fig. (1). It should be noted that charged scalars exist with the same masses as  $H_3^0$  and  $H_5^0$ .

The couplings of the neutral scalars to the fermions and the gauge bosons are

$$\begin{aligned} H_1^0 q\bar{q} &: -\frac{gm_q}{2m_W c_H}, & H_3^0 t\bar{t} &: \frac{igm_t s_H}{2m_W c_H} \gamma_5, & H_5^0 b\bar{b} &: -\frac{igm_b s_H}{2m_W c_H} \gamma_5, \\ H_1^0 W^+ W^- &: gm_W c_H, & H_1^0 Z Z &: \frac{g}{\cos^2 \theta_W} m_W c_H, \\ H_1^{0'} W^+ W^- &: \frac{2\sqrt{2}}{\sqrt{3}} gm_W s_H, & H_1^{0'} Z Z &: \frac{g2\sqrt{2}}{\cos^2 \theta_W \sqrt{3}} m_W s_H, \end{aligned}$$

$$H_5^0 W^+ W^- : \frac{1}{\sqrt{3}} g m_W s_H, \quad H_3^0 Z Z : -\frac{2g}{\cos^2 \theta_W \sqrt{3}} m_W s_H. \quad (12)$$

It is clear that, at tree-level, the coupling of the  $H_1^0$  to fermions is always enhanced by the factor of  $1/c_H$ . Conversely, the coupling of the  $H_3^0$  to fermions is either enhanced or suppressed, depending on the ratio of  $s_H$  and  $c_H$ , and the other neutral scalars do not couple to fermions. Importantly, the gauge boson couplings to  $H_1^0$  are suppressed by a factor  $c_H$  with respect to the SM and the role of vector boson fusion mechanism for  $H_1^0$  production is reduced if  $c_H$  is small. The other Higgs couplings to gauge bosons are suppressed by  $s_H$ . The  $Hq\bar{q}$  couplings presented in Fig. 2 (a) are considerably enhanced for small  $c_H$  in comparison to the SM prediction. In Fig. 2 (b), the  $HVV$  couplings are shown, again normalized to the SM couplings.

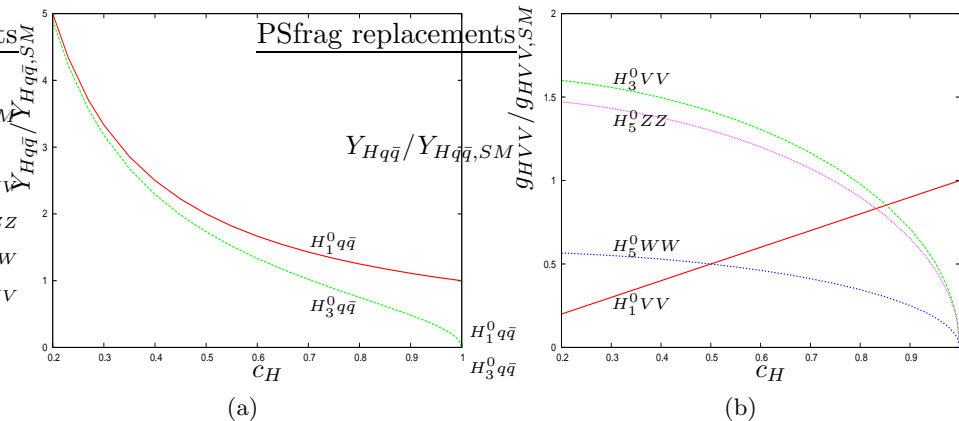


Figure 2: Couplings of the Higgs bosons to fermions (a) and gauge bosons (b), normalized by the Standard Model couplings.

### 3.2 Decays of $H_1^0$ and constraints on the parameters

In this section, we consider the  $H_1^0$  Higgs boson, which becomes the Standard Model Higgs boson for vanishing doublet-triplet mixing. The mass limits for  $H_1^0$  can be deduced from the LEP results. The couplings of the  $H_1^0$  to the gauge bosons are smaller than in the SM, leading to reduced production of Higgs bosons in Higgsstrahlung process [24], through which the Higgs was expected to be produced at LEP. The Higgs boson branching ratio to  $b\bar{b}$  is 74% for  $m_H = 114$  GeV in the Standard Model. Together with other fermions, the  $b\bar{b}$  decay mode gives the main contribution to the total width of the Higgs boson, and, thus, the Higgs branching ratio does not change very much with  $c_H$ : for  $m_H = 114$  GeV the branching ratio changes to 80% (81%) for  $c_H = 0.5$  ( $c_H = 0.2$ ). If the Higgs boson is lighter, the change is less. If we assume that the number of  $b$ -quark pairs gives the Higgs

boson mass limit, it must be heavier than 73 GeV (40 GeV) for  $c_H = 0.5$  ( $c_H = 0.2$ ). Unitarity further constrains most masses, requiring them to be less than of the order of 1 TeV [23, 25].

The Yukawa couplings are constrained by perturbativity, which limits the  $H_1^0$  coupling to top,

$$\frac{gm_{top}}{2m_W c_H} < \sqrt{4\pi}. \quad (13)$$

From this it follows that  $c_H > 0.2$ , which currently is the most stringent limit for  $c_H$ <sup>5</sup>. The latest 95% confidence limit for the cross section  $\times$  branching ratio of  $pp \rightarrow H \rightarrow \tau\tau$  for a 120 GeV Higgs boson is observed by the D0 Collaboration to be approximately 5 pb given 2.2 fb<sup>-1</sup> of data [27]. The CDF Collaboration observe a similar limit with 1.8 fb<sup>-1</sup> of data. Although this offers no sensitivity to a SM Higgs boson, which has a production cross section of  $\sim 1$  pb and a branching ratio of  $\sim 7\%$ , one would expect increased sensitivity for the  $H_1^0$  in the triplet model for small  $c_H$  (the production cross section is increased by a factor of  $1/c_H^2$  w.r.t to the SM as the main production channel would be gluon-gluon fusion via a top quark loop). Thus it seems likely that the final combined CDF/D0 results will further constrain the lower  $c_H$  limit given the expected integrated luminosity of 8 fb<sup>-1</sup> per experiment.

When calculating the branching ratios, it is necessary to consider also the loop induced decays of the Higgs bosons to gluons and photons. As mentioned, the tree-level gauge boson couplings to  $H_1^0$  are suppressed by a factor  $c_H$ . The  $\gamma\gamma H_1^0$  coupling is more complicated. In the SM, the W-loop gives the dominant contribution to the  $\gamma\gamma H$  coupling. In the triplet model however, the fermion coupling is enhanced and the W-coupling suppressed for small values of  $c_H$ , so that the top loop becomes more important and the  $\gamma\gamma H_1^0$  coupling is enhanced for small  $c_H$ . However, since the total width increases when  $c_H$  decreases, the branching ratio to photons remains smaller than in the SM. The gluon coupling to  $H_1^0$  is enhanced by  $1/c_H$  due to the fermion loop. These effects are seen in Fig. 3, where the branching ratios of  $H_1^0$  are presented for  $m_{H_1^0} = 120$  GeV and 150 GeV.

## 4 Central Exclusive Diffractive Production of the Triplet Higgs Boson

The central exclusive production (CEP) of a Higgs boson is defined as  $pp \rightarrow p \oplus H \oplus p$ , where the  $\oplus$  denote the presence of large rapidity gaps between

---

<sup>5</sup>Constraints from low energy precision measurements have been obtained from  $Zb\bar{b}$  vertex, meson-antimeson mixing and ratios of  $b \rightarrow u$  to  $b \rightarrow c$  decays [26]. The radiative corrections to the  $Zb\bar{b}$  vertex give the strongest constraint. Assuming  $m_{H_3} \sim 1$  TeV, one finds  $\cos\theta_H > 0.3$  with 99.9 % C.L. However, since we consider only tree-level results in this work, we have not used this bound.

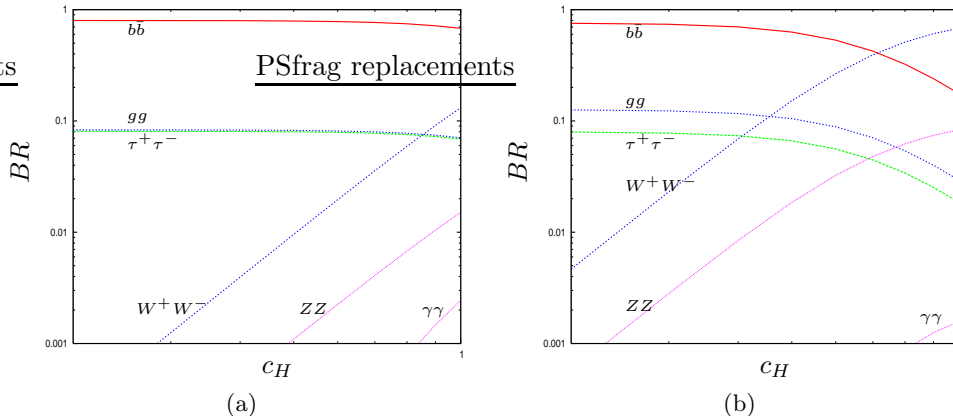


Figure 3: Branching ratios of  $H_1^0$  to the Standard Model particles for  $m_H = 120$  GeV (a) and  $m_H = 150$  GeV (b).

the outgoing protons and the decay products of the central system. It has been suggested in recent years that CEP offers a unique complimentary measurement to the conventional Higgs search channels, see for example, [7, 8], [28] - [33]. Firstly, if the outgoing protons scatter through small angles then, to a very good approximation, the primary active di-gluon system obeys a  $J_z = 0$ ,  $CP$ -even selection rule [34]. Here  $J_z$  is the projection of the total angular momentum along the proton beam axis. The observation of the Higgs boson in the CEP channel therefore determines the Higgs quantum numbers to be  $J^{PC} = 0^{++}$ . Secondly, because the process is exclusive, all of the energy/momentum lost by the protons during the interaction goes into the production of the central system. Measuring the outgoing proton allows the central mass to be measured to just a few GeV, regardless of the decay products of the central system. A mass measurement of this type will require new forward proton detectors to be installed at ATLAS and/or CMS, which we discuss further in section 5.1.

For a Standard Model Higgs boson, central exclusive diffraction could allow the main decay channels ( $b\bar{b}$ ,  $WW$  and  $\tau\tau$ ) to be observed in the same production channel, which provides the opportunity to study the Higgs coupling to  $b$ -quarks. This may be very difficult to access in other search channels at the LHC, despite the fact that  $H \rightarrow b\bar{b}$  is by far the dominant decay mode for a light SM Higgs boson. Furthermore, CEP can provide valuable information on the Higgs sector of MSSM, NMSSM and other popular BSM scenarios [35, 36, 31, 33, 37, 32]. In this paper, we propose that CEP is also beneficial if higher representations of the Higgs sector are realized, in particular, in searches for the Higgs triplets discussed in section 3.

The theoretical formalism [38] - [42] for central exclusive production contains distinct parts, as illustrated in Fig. 4. The cross section can be

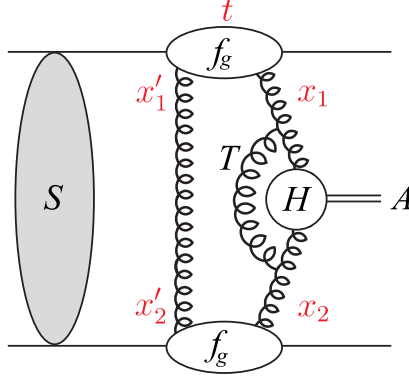


Figure 4: A symbolic diagram for the central exclusive production of a Higgs boson  $H$ .

written in the form [38, 7]

$$\sigma(pp \rightarrow p + H + p) \sim \frac{\langle S^2 \rangle}{B^2} \left| N \int \frac{dQ_t^2}{Q_t^4} f_g(x_1, x_1', Q_t^2, \mu^2) f_g(x_2, x_2', Q_t^2, \mu^2) \right|^2 \quad (14)$$

where  $B/2$  is the  $t$ -slope of the proton-Pomeron vertex,  $\langle S^2 \rangle$  is the soft-survival probability and the normalization,  $N$ , is given in terms of the  $H \rightarrow gg$  decay width. The amplitude-squared factor,  $|\dots|^2$ , can be calculated in perturbative QCD because the dominant contribution to the integral comes from the region  $\Lambda_{QCD}^2 \ll Q_t^2 \ll m_H^2$  for the large Higgs mass values of interest. The probability amplitudes,  $f_g$ , to find the appropriate pairs of  $t$ -channel gluons  $(x_1, x_1')$  and  $(x_2, x_2')$  are given by skewed unintegrated gluon densities at a hard scale  $\mu \sim m_H/2$ . It is important to emphasize, that these generalized gluon distributions are usually taken at  $p_t = 0$ , and then the “total” exclusive cross section is calculated by integrating over the transverse momentum,  $p_T$ , of the recoil protons. Assuming an exponential behaviour results in

$$\int dp_T^2 e^{-Bp_T^2} = 1/B = \langle p_T^2 \rangle. \quad (15)$$

Thus, the additional factor in Eq. (14) is not just the gap survival but rather the factor  $\langle S^2 \rangle/B^2$  [7, 43], which has the form  $S^2 \langle p_T^2 \rangle^2$  and is much less dependent on the parameters of the soft model [43, 41, 44]

The production cross section for Higgs bosons produced by gluon-gluon fusion and decaying to  $b\bar{b}$  is proportional to

$$\frac{\Gamma^{\text{eff}}}{m_H^3} \equiv \frac{\Gamma(H \rightarrow gg)}{m_H^3} BR(H \rightarrow b\bar{b}) \quad (16)$$

|             | $m_H = 120 \text{ GeV}$    |                                     | $m_H = 150 \text{ GeV}$    |                                     |
|-------------|----------------------------|-------------------------------------|----------------------------|-------------------------------------|
|             | $\Gamma(H \rightarrow gg)$ | $\text{BR}(H \rightarrow b\bar{b})$ | $\Gamma(H \rightarrow gg)$ | $\text{BR}(H \rightarrow b\bar{b})$ |
| $c_H = 0.2$ | $6.35 \times 10^{-3}$      | 0.80                                | $1.22 \times 10^{-2}$      | 0.75                                |
| $c_H = 0.5$ | $1.01 \times 10^{-3}$      | 0.79                                | $1.95 \times 10^{-3}$      | 0.63                                |
| $c_H = 0.8$ | $3.97 \times 10^{-4}$      | 0.74                                | $7.63 \times 10^{-3}$      | 0.32                                |
| SM          | $2.49 \times 10^{-4}$      | 0.68                                | $4.79 \times 10^{-4}$      | 0.18                                |

Table 1: The  $H_1^0$  partial decay width to gluons (expressed in GeV) and branching ratio to  $b\bar{b}$  for specific values of Higgs mass and  $c_H$ . The Standard Model (SM) prediction is shown for comparative purposes.

where  $\Gamma(H \rightarrow gg)$  is the decay width to gluons and  $\text{BR}(H \rightarrow b\bar{b})$  is the branching ratio to  $b\bar{b}$  quarks. Table 1 shows the value of these parameters for the SM Higgs and the lightest Higgs,  $H_1^0$ , in the triplet model. The central exclusive  $H \rightarrow b\bar{b}$  cross section can therefore be enhanced by a large factor with respect to the Standard Model - we discuss this further in Section 5

The CEP formalism has been extensively checked using the diffractive production of  $J/\psi$  and the leading neutron spectra [45] at HERA and the CDF data on central exclusive production processes [46] - [48]. Further tests of the formalism using the early LHC data have also been suggested [42]. The main uncertainties are associated with:

- The probability  $\langle S^2 \rangle$  that additional secondaries will not populate the gaps.
- The probability to find the appropriate gluons that are given by generalized, unintegrated distributions  $f_g(x, x', Q_t^2)$ .
- Higher order QCD corrections to the hard subprocess, in particular, the Sudakov suppression.
- The so-called ‘enhanced absorptive corrections’ [49, 50, 41] and other effects that may violate the soft-hard factorization.

Let us focus first on the gap survival factor  $\langle S^2 \rangle$ . Since soft physics is involved, we need a reliable model of soft interactions to quantify the role of the absorption effects. In [39, 40, 41] soft interaction models were developed and tuned to describe all the available high energy soft  $pp$  interaction data. These models account for (i) elastic rescattering (with the two protons in intermediate states), (ii) the probability of low-mass proton excitations, and (iii) the screening corrections due to high-mass proton dissociation (enhanced absorption). The first two effects result in the so-called eikonal contribution,  $\langle S_{\text{eik}}^2 \rangle$ . In the most recent version of the soft rescattering model [41, 44], the KMR group obtained  $\langle S_{\text{eik}}^2 \rangle_{\text{eff}} = 0.025$  when adjusting  $\langle S_{\text{eik}}^2 \rangle$  to its value corresponding to an exponential slope  $B = 4 \text{ GeV}^{-2}$ .

In the presence of enhanced screening, however, there is no longer exact factorisation between the hard and soft parts of the process, see for example [50, 45, 41]. The latest calculations [41] indicate that, in the case of the SM Higgs production at the LHC, the effective survival factor, due to both eikonal and enhanced rescattering, is  $\langle S^2 \rangle_{\text{eff}} \simeq 0.015 \pm 0.01$ . It should be noted that the exclusive dijet,  $\gamma\gamma$  and  $\chi_c$  production data from CDF and the leading neutron data at HERA indicate that  $\langle S_{\text{enh}}^2 \rangle$  is somewhat larger than this estimate, such that  $\langle S^2 \rangle_{\text{eff}}$  is nearer the upper limit of the quoted interval. In any case, it will be possible to measure  $\langle S_{\text{enh}}^2 \rangle$  using early LHC data [42, 51].

As the generalized, unintegrated gluon distribution  $f_g$  has not been measured explicitly, it is obtained in the KMR approach [38, 7] from the conventional gluon distribution,  $g(x, Q_t^2)$ , known from the global parton analyses. The main uncertainty comes from the lack of knowledge of the integrated gluon distribution at low  $x$  and small scales. It was found in [42] that a variety of recent global analyses give a spread of

$$xg = (3 - 3.8) \text{ for } x = 10^{-2} \quad \text{and} \quad xg = (3.4 - 4.5) \text{ for } x = 10^{-3} \quad (17)$$

for  $Q_t^2 = 4 \text{ GeV}^2$ . These are big uncertainties bearing in mind that the CEP cross section depends on  $(xg)^4$ . A similar estimate of the uncertainty from the input gluon distribution functions was presented in [33]. The uncertainty related to the Sudakov factor is addressed in [42], along with the measurements that could reduce the uncertainty using early LHC data.

The overall uncertainty factor in the calculation of the CEP of Higgs bosons at the LHC was estimated to be approximately 2.5 in [35, 31]. Again, we note that the first LHC runs will allow the accuracy to be drastically improved.

## 5 Simulation of Higgs production in the triplet model

### 5.1 Forward proton tagging

The forward proton detectors will need to be installed in the high dispersion regions 220 m and 420 m either side of the interaction point at ATLAS and/or CMS<sup>6</sup>. We restrict our discussion and analysis to the ATLAS interaction point (IP), and note that a similar result would be obtained at CMS. There are three important aspects of forward proton tagging at the LHC that need to be considered for the purposes of this analysis; the acceptance and resolution of the proposed forward proton detectors and the ability of the detectors to measure the time-of-flight of each proton from the interaction point.

---

<sup>6</sup>We refer the reader to the FP420 R&D report for more details on the detectors [8].

The acceptance of the forward proton system depends on the distance that each active detector is from the LHC beam. We choose the proton detectors located at 220 m (420 m) from the IP to be 2 mm (5 mm) from the beam and use the FPtrack program [52] to track the path of the protons through the LHC lattice in order to fully determine the acceptance. The acceptance of the forward proton detector system is dependent on the mass of the centrally produced object,  $M$ , which is given by

$$M^2 = \xi_1 \xi_2 s \quad (18)$$

where  $\xi_1$  and  $\xi_2$  are the fractional longitudinal momentum losses of the outgoing protons. For central masses less than 200 GeV, the protons are either both detected at 420m (symmetric tagging) or one is detected at 220 m and one at 420 m (asymmetric tagging). For example, the acceptance for a central mass of 120 GeV is approximately 28% for symmetric events and 20% for asymmetric events<sup>7</sup> [8]. This acceptance changes to 20% and 40% respectively for a 150 GeV central mass. Furthermore, symmetric and asymmetric events also have different mass resolution for a given central mass; the resolution of a 150 GeV Higgs boson is approximately 1.5 GeV and 4 GeV for symmetric and asymmetric proton tagging respectively.

Finally, the forward proton detectors will be capable of measuring the time-of-flight of each proton from the interaction point to an accuracy of 10 ps. The difference in the time-of-flight measurement of the protons gives a measurement of the interaction vertex to 2.1 mm, assuming that the reference timing system has negligible jitter. This vertex reconstruction proves to be very useful in background rejection, as discussed in Section 5.3.

## 5.2 Signal and background event generation

The central exclusive signal and background events are simulated with full parton showering and hadronization effects using the ExHuME v1.3.4 event generator [53]. ExHuME contains a direct implementation of the KMR calculation [38, 7] of central exclusive diffraction given in Sec. 4. The CTEQ6M [54] parton distribution functions are used to calculate the generalized gluon distributions,  $f_g$ . The generator level cross sections for central exclusive  $H \rightarrow b\bar{b}$  production in the triplet model are presented in Table 2 for  $m_H = 120, 150$  GeV and  $c_H = 0.2, 0.5, 0.8$ . In Section 5.5 we will present results for each of these parameter choices.

The backgrounds to  $H \rightarrow b\bar{b}$  can be broken down into three broad categories; central exclusive, double pomeron exchange and overlap. We use the ExHuME event generator for the central exclusive backgrounds. ExHuME contains the leading order calculation for central exclusive  $b\bar{b}$  production.

---

<sup>7</sup>Dead material in the detectors at 220 m can reduce the acceptance for symmetric tagging. We do not consider that effect here.

| $\sigma_{H \rightarrow b\bar{b}}$ (fb) | $m_H = 120$ GeV | $m_H = 150$ GeV |
|--|-----------------|-----------------|
| $c_H = 0.2$                            | 113.5           | 55.2            |
| $c_H = 0.5$                            | 18.0            | 7.4             |
| $c_H = 0.8$                            | 6.6             | 1.5             |

Table 2: Generator level cross sections,  $\sigma_{H \rightarrow b\bar{b}}$ , for central exclusive Higgs boson production for  $m_H = 120, 150$  GeV and  $c_H = 0.2, 0.5, 0.8$ .

Recent results however [55], show that the one-loop corrections to this process reduce the cross section by a factor of approximately two. We normalize the  $b\bar{b}$  events generated by ExHuME accordingly. Central exclusive  $gg$  production has a much larger cross section than  $b\bar{b}$  and can act as a background when the gluon jets are mis-identified by the b-tagging algorithms. At ATLAS, the mis-identification rate for each gluon jet is 1.3% for a b-tagging efficiency of 60% [56]. We do not generate exclusive  $c\bar{c}$  events for two reasons. Firstly, due to the  $J_z = 0$  spin-selection rule [34], exclusive  $c\bar{c}$  production is suppressed with respect to  $b\bar{b}$  by a factor of  $m_c^2/m_b^2$ . Furthermore, the mis-tag rate for c-jets to be identified as b-jets is  $\sim 10\%$ . Thus, the background contribution from exclusive  $c\bar{c}$  events is considered to be negligible in comparison to the exclusive  $b\bar{b}$  events. Higher order events, such as  $b\bar{b}g$  have been studied in [57] with the conclusion that these types of events should be negligible after all experimental cuts. The demonstration of this using event generators cannot be completed until the relevant processes are implemented into the ExHuME Monte Carlo.

Double pomeron exchange (DPE) is the process  $pp \rightarrow p+X+p$ , where the central system,  $X$ , is produced by pomeron-pomeron fusion. The pomeron is assigned a partonic structure and so there are always ‘pomeron remnants’ accompanying the hard scatter. DPE has been extensively studied in relation to  $H \rightarrow b\bar{b}$  and it has been concluded that this background is negligible after appropriate experimental cuts [33, 58]. We do not consider these types of events further.

In addition to these standard backgrounds, we also examine the effect of the overlap backgrounds. This source of background is important when there are a large number of  $pp$  interactions in each bunch crossing at the LHC. The largest overlap background is a three-fold coincidence between two soft events ( $pp \rightarrow pX$ ), which produce forward protons within the acceptance of the forward detectors, and an inelastic event, which produces the hard scatter  $pp \rightarrow X$  and, thus, can mimic our signal. To simulate these events we use HERWIG [59] plus JIMMY [60] to generate  $pp \rightarrow b\bar{b}$ , using the tune (A) to Tevatron data [61]. The forward protons are then added into the event using the prescription given in [33], which also allows us to calculate the probability of the coincidence as a function of the LHC luminosity.

The overlap background is initially reduced using the vertex matching

provided by the proton time-of-flight (TOF) information. As the protons do not come from the same interaction as the jets, the vertex reconstructed using TOF will not, in general, coincide with the di-jet vertex. Given a fast-timing resolution of 10 ps, a rejection factor of 18 (15) can be obtained at low (high) luminosity by requiring that the di-jet vertex be within  $\pm 4.2$  mm of the ‘fake’ vertex reconstructed from TOF. Approximately 95% of the CEP events will be retained by this requirement.

We do not consider the backgrounds from two-fold coincidences. It was demonstrated in [33] that the largest of these backgrounds - the coincidence between a soft central diffractive scattering and a standard QCD  $2 \rightarrow 2$  scattering - was at least a factor of five smaller than the threefold coincidence. Furthermore, as discussed in the FP420 R&D report [8], this background is (i) probably overestimated and (ii) will be additionally rejected by the charged track cut outlined in the next section.

When generating the event samples, we require that the central mass be in the range  $80 < M < 250$  GeV, which improves the event generator efficiency and is the broad region of interest for this study. To approximate the detector effects, we smear the energy, momenta and angles of each central final state particle according to the ATLAS detector resolution [62]. The outgoing forward proton momenta are smeared by the amount specified in [63]. A mid-point cone algorithm is then applied to the samples and events retained if the leading jet has transverse energy greater than 45 GeV. Finally, b-tagging efficiencies are imposed after matching the two leading jets to the partonic level.

### 5.3 Experimental cuts

To enhance the signal, we follow the experimental method used in a previous study of  $H \rightarrow b\bar{b}$  in the SM and the MSSM [33], which imposes a number of exclusivity cuts<sup>8</sup>. Firstly, the rapidity of the central system can be estimated from the forward proton detectors by

$$y = \frac{1}{2} \ln \left( \frac{\xi_1}{\xi_2} \right). \quad (19)$$

The difference,  $\Delta y$ , between this rapidity measurement and the average pseudo-rapidity of the di-jets should be approximately zero for an exclusive event, Exclusive candidates satisfy

$$\Delta y = \left| y - \left( \frac{\eta_1 + \eta_2}{2} \right) \right| \leq 0.06, \quad (20)$$

where  $\eta_1$  and  $\eta_2$  are the pseudo-rapidities of the leading jets.

---

<sup>8</sup>A somewhat different experimental method was discussed in [31]. However, the final experimental efficiency broadly agrees with that used here [8].

The di-jet mass fraction,  $R_j$ , determines the fraction of the central mass that is contained within the di-jet system.  $R_j$  is an improved version of the  $R_{jj}$  variable [64], which was used by CDF in the search for exclusive di-jet events [46]. For an exclusive di-jet event, one expects all of the mass to be contained in the di-jets, and hence  $R_j = 1$ . However, parton showering/hadronisation effects can result in energy outside of the jets. Furthermore, detector resolution will smear the di-jet mass measurement. An exclusive event is defined to be

$$0.85 \leq R_j = \frac{2E_T^1}{M} \cosh(\eta_1 - y) \leq 1.1, \quad (21)$$

where  $E_T^1$  is the transverse energy of the leading jet.

The third exclusivity cut requires the di-jets to be back to back in azimuth, which reflects the suppression of initial state radiation for an exclusive di-jet event. The back to back requirement is

$$|\pi - \Delta\phi| \leq 0.15, \quad (22)$$

where  $\Delta\phi$  is the azimuthal angle between the jets. It is also possible to examine each event for underlying event activity, caused by multiple parton-parton interactions. The exclusive events do not have these additional scatterers because the proton remains intact. It is possible to reject inclusive events, and, hence, the overlap background, by requiring few charged tracks,  $N_C$ , associated with the di-jet vertex but outside of the jets. This definition is, of course, dependent on the jet algorithm used to define the jets. An algorithm independent approach is to examine the charged track activity perpendicular to the leading jet,  $N_C^\perp$ . In this approach, charged tracks are assigned to the underlying event if they satisfy

$$\frac{\pi}{3} \leq |\phi_k - \phi_1| \leq \frac{2\pi}{3} \quad \text{or} \quad \frac{4\pi}{3} \leq |\phi_k - \phi_1| \leq \frac{5\pi}{3}, \quad (23)$$

where  $\phi_k$  is the azimuthal angle of a charged track and  $\phi_1$  is the azimuthal angle of the leading jet. In this analysis, we identify exclusive events by

$$N_C \leq 3 \quad \text{and} \quad N_C^\perp \leq 1. \quad (24)$$

For completeness, in Table 3 we present the final cross sections for the signal ( $m_H = 120$  GeV,  $c_H = 0.5$ ) and background events. It should be noted that the signal is concentrated at  $M = 120$  GeV, whereas the backgrounds form a continuum across the mass range  $80 < M < 250$  GeV. For details on the efficiencies of the individual cuts, and motivation for the cut choices, we refer the reader to [33]. The overlap backgrounds are luminosity dependent and are presented for constant luminosities of  $10^{33} \text{ cm}^{-2} \text{ s}^{-1}$  (low) and  $10^{34} \text{ cm}^{-2} \text{ s}^{-1}$  (high).

| Generator      | Process                  | $\sigma_{420-420}$ (fb) | $\sigma_{420-220}$ (fb) |
|----------------|--------------------------|-------------------------|-------------------------|
| ExHuME         | $H \rightarrow b\bar{b}$ | 0.53                    | 0.28                    |
|                | $b\bar{b}$               | 0.53                    | 0.27                    |
|                | $g\bar{g}$               | 1.08                    | 0.91                    |
| Overlap (L)    | $b\bar{b}$               | 0.07                    | 0.09                    |
| Overlap (H)    | $b\bar{b}$               | 11.0                    | 13.7                    |
| Total bgrd (L) |                          | 1.68                    | 1.27                    |
| Total bgrd (H) |                          | 12.6                    | 14.9                    |

Table 3: The final cross sections for the  $H \rightarrow b\bar{b}$  ( $m_H = 120$  GeV,  $c_H = 0.5$ ) and relevant backgrounds after the all cuts discussed in the text. The overlap backgrounds are defined at both low (L) and high (H) luminosity. All the backgrounds form a continuum over the range  $80 < M < 250$  GeV.

#### 5.4 Trigger strategies

A major experimental challenge for central exclusive jet analyses is developing a trigger strategy to retain enough events. At ATLAS, jets with  $E_T \sim 50$  GeV are heavily prescaled in the level one (L1) trigger, due to the high rate and the lack of additional rejective power in the high level trigger (HLT). The total L1 rate allowed at ATLAS is 75-100 kHz, which must be reduced to  $\sim 100$  Hz after the HLT. In this section, we discuss three possible trigger strategies. The first possibility is to exploit the muon rich nature of  $b\bar{b}$  events. The lowest muon threshold (MU6) at ATLAS is designed to retain 80% of muons with transverse momentum greater than 6 GeV. The single muon trigger efficiency for  $b\bar{b}$  events is 11% [33]. In order to keep the L1 rate down it will be necessary to require that the event contains jet with  $E_T > 40$  GeV in conjunction with the muon.

The second trigger strategy is to require a 40 GeV jet in conjunction with a proton tagged in a detector at 220 m from the interaction point<sup>9</sup>. This trigger has been extensively studied in previous work [65], and it is expected that the unprescaled L1 rate will be less than 1 kHz up to a luminosity of  $L=2 \times 10^{33}$  cm<sup>-2</sup> s<sup>-1</sup>. This rate however, will scale with  $L^2$  and the trigger may have to be prescaled to give a fixed rate at the highest luminosity. We will investigate two fixed rate triggers; R5 is a L1 rate of 5 kHz and R10 is a L1 rate of 10 kHz. The drawback of this trigger strategy is that the symmetric events will not be retained, which could potentially have a large impact for a light Higgs boson measurement.

It will be possible to dramatically reduce any high L1 rate using additional information in the HLT. Firstly, requiring that there be a proton detected at 420 m and using time-of-flight information to match the vertices

<sup>9</sup>The information from the detectors at 420m will not reach the central trigger processor within the latency of  $2.5\mu\text{s}$  and so cannot be used in the L1 decision.

will reject the events by a factor of approximately 600 (60) at low (high) luminosity. A loose b-tagging requirement could also be added. Finally, the  $R_j$  and  $\Delta y$  cuts reject the overlap events by a factor of approximately 100 and could be used to further reduce the rate.

The final trigger strategy is to allow a larger L1 rate for the 40 GeV jets, which is then reduced in the HLT by requiring two in-time protons. This trigger has also been studied in previous work [33]. The advantage of this approach is that it would retain both symmetric and asymmetric events. The L1 rate for 40 GeV jets is expected to be approximately 25 kHz at low luminosity, rising to 250kHz at high luminosity. We define a trigger for 40 GeV jets, JR25, which has a fixed rate of 25 kHz<sup>10</sup>. This trigger would be unrescaled at low luminosity and prescaled by a factor of ten at high luminosity.

## 5.5 Significance of observation and expected mass distributions

In this section, we estimate the significance of observing a neutral Higgs boson in the triplet model for the parameter choices presented in section 5.2 and for the trigger strategies outlined in section 5.4. As the overlap background is luminosity dependent (Table 3), we must specify how the data was collected. For example, we examine the significance for an integrated luminosity of 60 fb<sup>-1</sup>, which corresponds to between three and four years of data acquisition given a peak luminosity of  $2 \times 10^{33}$  cm<sup>-2</sup> s<sup>-1</sup>. We also present results for 300 fb<sup>-1</sup> of data, which corresponds to between three and four years of data acquisition given a peak luminosity of  $10^{34}$  cm<sup>-2</sup> s<sup>-1</sup>. It should be noted, however, that the data acquisition at the LHC will not be collected at one specific luminosity. Firstly, the peak luminosity will increase during the lifetime of the LHC with an improved understanding of the machine. Secondly, during each store, the luminosity will decrease exponentially with a lifetime of approximately 14 hours. We crudely approximate these effects by defining that half the data is collected at the peak luminosity and half the data at 75% of the maximum.

The signal and background events that pass the selection criteria are normalized to an expected number,  $N$ , for each trigger/luminosity scenario, i.e.

$$N = L\sigma\epsilon,$$

where  $L$  is the total integrated luminosity,  $\sigma$  is the final cross section for each process as shown in Table 3 and  $\epsilon$  is the trigger efficiency. In the case of the overlap background,  $\sigma$  is dependent on the assumed peak luminosity

---

<sup>10</sup>It was shown in CMS-based study [66] that this rate can be reduced by a factor of two by requiring that the majority of the transverse energy in the detector be contained within the dijets - i.e. that  $(E_T^1 + E_T^2)/H_T > 0.9$ , where  $H_T$  is the scalar sum of transverse energy deposited in the detector [65].

as described above. The MC distributions are then used to predict the expected number of events in each bin of a mass distribution. A pseudo-experiment is then carried out by randomly picking a number of events for each bin in the mass distribution according to a Poisson distribution. The significance of each pseudo-experiment is then obtained by fitting the pseudo-data with a signal-plus-background function and a background-only function. The significance is estimated from the difference in  $\chi^2$  of the two fits by

$$S = \sqrt{\chi_b^2 - \chi_{s+b}^2}. \quad (25)$$

We assume the background function will be well known from data - in this analysis we use the weighted MC background events to determine the shape and allow the normalization to vary<sup>11</sup>. The signal function is a Gaussian and all parameters are allowed to vary. We repeat the procedure for 500 pseudo-experiments to determine the average significance of each luminosity/trigger scenario and ensure that our results are consistent and the presented distributions typical.

To determine the significance for each parameter choice, the trigger strategies outlined in Sec 5.4 are evaluated and the best method chosen to retain the events. We choose the  $m_H = 120$  GeV,  $c_H = 0.5$  point as our reference. Figure 5 (a) shows the significance as a function of luminosity for the R5, R10 and JR25 trigger strategies given three years of data acquisition at that luminosity. It is clear that the JR25 trigger is the best choice at low luminosity as it retains a high fraction of both symmetric and asymmetric events. At higher luminosities, the R5/R10 triggers become more favourable; the R5 (R10) trigger do not become prescaled until  $4.5 \times 10^{33} \text{ cm}^{-2} \text{ s}^{-1}$  ( $6.3 \times 10^{33} \text{ cm}^{-2} \text{ s}^{-1}$ ) and the number of exclusive events in the final sample is increased even though the symmetric events are not retained. Figure 5 (b) shows the significance for R5, R10 and JR25 when combined with the MU6 trigger.

Figure 6 shows the expected mass distributions for  $m_H = 120, 150$  GeV and  $c_H = 0.2, 0.5$  for  $60 \text{ fb}^{-1}$  of data collected at  $2 \times 10^{33} \text{ cm}^{-2} \text{ s}^{-1}$  using a JR25+MU6 trigger. Example distributions for  $c_H = 0.8$  are not shown as the calculated significance is less than  $3\sigma$ . Figure 7 shows the same distributions but for  $300 \text{ fb}^{-1}$  of data collected at  $10^{34} \text{ cm}^{-2} \text{ s}^{-1}$  using the R10+MU6 trigger. A summary of the significance for each parameter choice is presented in Table 4 for both luminosity/trigger scenarios. The significance is approximately  $4\sigma$  for the  $c_H = 0.5$  parameter points and  $12\sigma$  for the  $c_H = 0.2$  parameter points.

For each parameter point, the information obtained from the fitting procedure in each pseudo-experiment can be used to obtain an RMS spread of Higgs masses. This gives a reasonable estimate of the error on the Higgs mass

---

<sup>11</sup>We have checked our results using a quadratic background function and observe little difference.

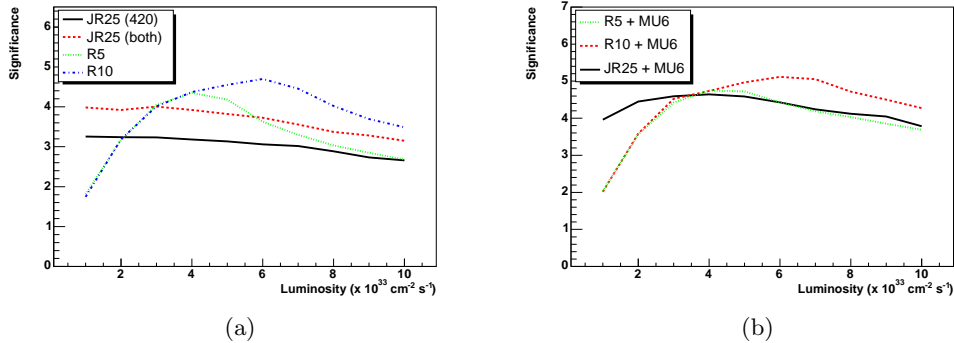


Figure 5: (a) Expected significance ( $m_H = 120 \text{ GeV}$ ,  $c_H = 0.5$ ) for the R5, R10 and JR25 triggers as a function of luminosity given three years of data acquisition at each luminosity. We assume that  $10 \text{ fb}^{-1}$  of data is collected each year per  $10^{33} \text{ cm}^{-2} \text{ s}^{-1}$  of luminosity, i.e.  $120 \text{ fb}^{-1}$  of data is collected at  $4 \times 10^{33} \text{ cm}^{-2} \text{ s}^{-1}$ . (b) The significance of the R5, R10 and JR25 triggers when combined with the MU6 trigger.

as measured by the forward proton detectors. Table 5 shows the RMS spread for each (significant) parameter choice. The R10 trigger strategy (used at high luminosity) retains only events with asymmetrically tagged protons, whereas the JR25 trigger (used at low luminosity) retains both symmetric and asymmetric events. Thus the high luminosity scenario in Table 5 results in a poorer mass measurement than the low luminosity scenario because of the lower fraction of symmetric events in the sample. The final trigger strategy at ATLAS/CMS will have to balance the need for observation with the opportunity for more precise measurements. For all parameter choices the mass measurement can be made to better than  $2 \text{ GeV}$ ; for  $c_H = 0.2$  the mass measurement is better than  $0.3 \text{ GeV}$ .

It should be noted that the significances obtained for the  $c_H = 0.2$  parameter points are well in excess of  $10\sigma$  and the high rate triggers assumed in this analysis are not strictly needed for the measurement. Indeed, the MU6 trigger alone is capable of retaining enough events for the analysis - the significance for a  $120 \text{ GeV}$  Higgs boson is  $4.5$  for  $60 \text{ fb}^{-1}$  collected at  $2 \times 10^{33} \text{ cm}^{-2} \text{ s}^{-1}$ . The disadvantage is that the mass measurement is somewhat degraded, due to the reduced number of events.

The  $c_H = 0.8$  points are observable if the overlap background can be additionally rejected. There are two possibilities related to improvements in the fast-timing system. Firstly, if the time-of-flight resolution of the forward detectors is improved, then both the vertex resolution and overlap rejection is improved by the same factor. Secondly, if the central jets can be timed to an accuracy of  $70 \text{ ps}$ , using optimal signal filtering in the ATLAS Liquid Argon Calorimeter [67], a factor of two rejection on the overlap background

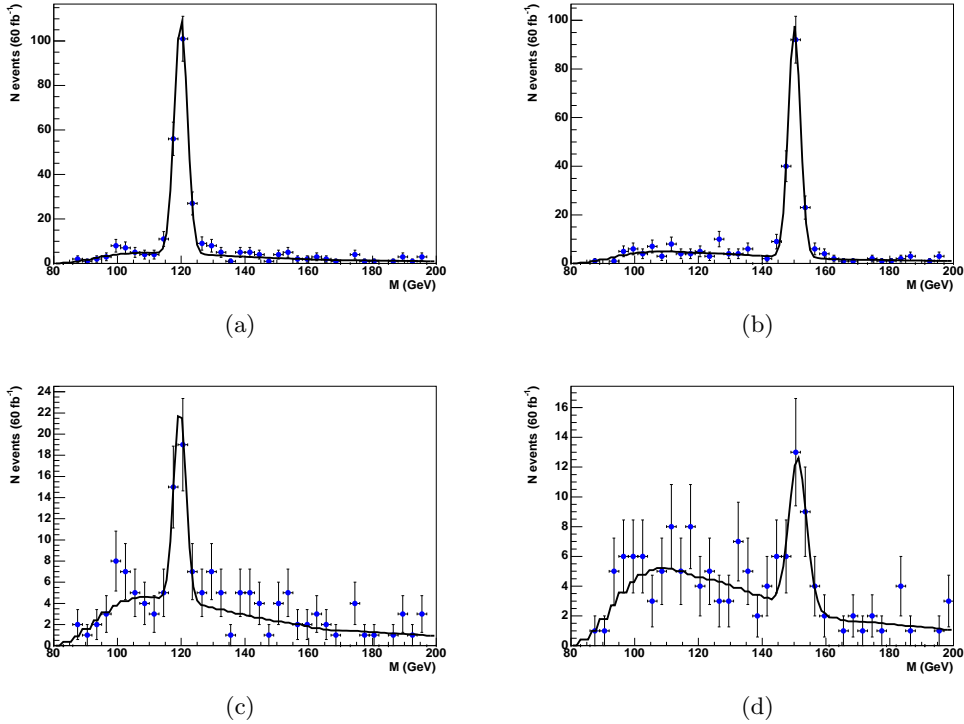


Figure 6: Expected mass distributions given  $60 \text{ fb}^{-1}$  of data, collected at  $2 \times 10^{33} \text{ cm}^{-2} \text{ s}^{-1}$  using a JR25+MU6 trigger, for the following parameter choices: (a)  $m_H = 120 \text{ GeV}$  and  $c_H = 0.2$ , significance is  $12.7\sigma$  (b)  $m_H = 150 \text{ GeV}$  and  $c_H = 0.2$ , significance is  $11.9\sigma$ . (c)  $m_H = 120 \text{ GeV}$  and  $c_H = 0.5$ , significance is  $4.5\sigma$ . (d)  $m_H = 150 \text{ GeV}$  and  $c_H = 0.5$ , significance is  $3.9\sigma$ .

would be gained. If the central timing could be performed at the 10 ps level, then a factor of 12 rejection would be observed. The significance of the  $c_H = 0.8$  parameter point for a 120 GeV Higgs boson increases to  $3.2\sigma$  at high luminosity if the overlap background is additionally rejected by a factor of five. Improved overlap rejection would also increase the significance of the other parameter points at high luminosity.

## 6 Doubly charged Higgs bosons

An important feature of the triplet model is the existence of doubly charged Higgs bosons. Although not the focus of this paper, we comment on the possibility to observe these using the forward proton system discussed in section 5.1. The process of interest is  $pp \rightarrow p \oplus H^{++}H^{--} \oplus p$ , where the central system is produced via photon-photon fusion, *i.e.*  $\gamma\gamma \rightarrow H^{++}H^{--}$ .

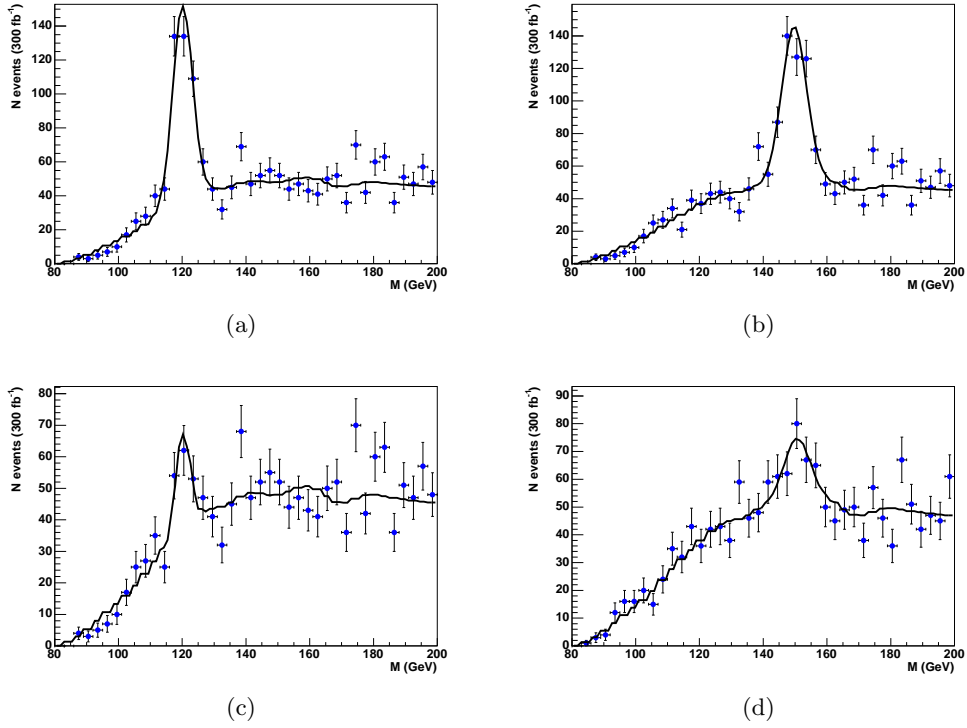


Figure 7: Expected mass distributions given  $300 \text{ fb}^{-1}$  of data, collected at  $10^{34} \text{ cm}^{-2} \text{ s}^{-1}$  using a R10+MU6 trigger for the following parameter choices (a)  $m_H = 120 \text{ GeV}$  and  $c_H = 0.2$ , significance is  $13.7\sigma$  (b)  $m_H = 150 \text{ GeV}$  and  $c_H = 0.2$ , significance is  $12.7\sigma$ . (c)  $m_H = 120 \text{ GeV}$  and  $c_H = 0.5$ , significance is  $4.3\sigma$ . (d)  $m_H = 150 \text{ GeV}$  and  $c_H = 0.5$ , significance is  $4.3\sigma$ .

| $m_H$ (GeV) | $c_H$ | Significance ( $\sigma$ ) |                      |
|-------------|-------|---------------------------|----------------------|
|             |       | 60 fb <sup>-1</sup>       | 300 fb <sup>-1</sup> |
| 120         | 0.2   | 12.7                      | 13.7                 |
|             | 0.5   | 4.5                       | 4.3                  |
|             | 0.8   | 2.6                       | 2.5                  |
| 150         | 0.2   | 11.9                      | 12.7                 |
|             | 0.5   | 3.9                       | 4.3                  |
|             | 0.8   | 2.0                       | 2.1                  |

Table 4: Significance of central exclusive Higgs boson measurement for  $m_H = 120, 150$  GeV and  $c_H = 0.2, 0.5, 0.8$ . The significance is obtained after using the cuts, trigger strategies and fitting procedure outlined in the text. As the overlap background is luminosity dependent, we present results for both 60 fb<sup>-1</sup> of data taken at a peak luminosity of  $2 \times 10^{33}$  cm<sup>-2</sup> s<sup>-1</sup> and for 300 fb<sup>-1</sup> of data taken at a peak luminosity of  $10^{34}$  cm<sup>-2</sup> s<sup>-1</sup>.

| $m_H$ (GeV) | $c_H$ | $\sigma_{m_H}$ (GeV) |                      |
|-------------|-------|----------------------|----------------------|
|             |       | 60 fb <sup>-1</sup>  | 300 fb <sup>-1</sup> |
| 120         | 0.2   | 0.2                  | 0.3                  |
|             | 0.5   | 0.8                  | 4.5                  |
| 150         | 0.2   | 0.2                  | 0.3                  |
|             | 0.5   | 1.8                  | 2.4                  |

Table 5: The error in the Higgs boson mass measurement,  $\sigma_{m_H}$ , estimated from the RMS spread of mass measurements made in the pseudo-experiments, for  $m_H = 120, 150$  GeV and  $c_H = 0.2, 0.5$ . The 60 fb<sup>-1</sup> of data (taken at a peak luminosity of  $2 \times 10^{33}$  cm<sup>-2</sup> s<sup>-1</sup>) uses a JR25 + MU6 trigger strategy whereas the 300 fb<sup>-1</sup> of data (taken at a peak luminosity of  $10^{34}$  cm<sup>-2</sup> s<sup>-1</sup>) uses R10 + MU6.

As two Higgs bosons are produced, the central system will be of higher mass than discussed in previous sections and at least one of the protons will be tagged by detectors placed at 220m from the IP.

The production cross section could be large [68]. It was shown in [69, 8] that the production cross section was 0.07 fb for a 200 GeV for singly charged scalar pair production. However, the cross section for doubly charged Higgs boson<sup>12</sup> pair production is a factor of 16 larger due to the factor of two increase in charge. Thus the cross section for pair-production of a 200 GeV doubly charged Higgs boson increases to 1.1 fb. It should be noted that the photon fusion production cross section decreases roughly by  $\sim 1/M^3$  [7], and so the pair production of a 300 GeV doubly charged scalar would be

<sup>12</sup>The doubly charged Higgs boson mass in the Machacek-Georgi model is the same as the  $H_3^0$  scalar mass, and therefore,  $H^{++}$  with mass  $m_{H^{++}} \sim 200 - 300$  GeV is possible, as it is heavier than the lightest neutral Higgs  $H_1^0$ .

approximately 0.3 fb.

The forward proton acceptance for central systems in the range 400 GeV-1 TeV is better than 40% [63]. This means that we would expect more than 130 events with both outgoing protons measured for the pair production of a 200 GeV doubly charged Higgs boson given  $300 \text{ fb}^{-1}$  of data acquisition. This decreases to 40 events if the mass of the doubly charged Higgs is 300 GeV.

The events should be retained using the standard electron/muon trigger strategies currently in place at ATLAS/CMS. A doubly charged Higgs that is heavier than 200 GeV has several possible decay modes:  $H^{++} \rightarrow W^+W^+$ ,  $W^+H^+$ ,  $H^+H^+$ ,  $l^+l^+$ . In any case, a high fraction of events will contain at least one electron/muon in the final state.

Therefore, forward proton tagging allows the possibility to study doubly charged scalars that are lighter than around 300 GeV. Note that, in exclusive production, the background conditions are more favourable in comparison to the conventional  $pp \rightarrow H^{++}H^{--}X$  case considered *e.g.* in [68]. Also, in principle, the forward proton mode may allow to measure the  $H^{\pm\pm}$  mass more accurately than in the inclusive case.

## 7 Conclusions

Searches for the manifestation of the extended Higgs sector at the LHC may allow new insight in the nature of electroweak symmetry breaking. The central exclusive production mechanism would provide a very powerful tool to complement the standard strategies at the LHC for studying Higgs particles. Here we focus on the production of the neutral Higgs boson of the triplet model in the forward proton mode. We assume a model with the tree-level value of the electroweak  $\rho$ -parameter consistent with experiment,  $\rho = 1$ . Although this model is used as a benchmark model for the triplets, our results are more general. An extra contribution from other representations enhances the doublet Yukawa couplings resulting in a different experimental signature to that of the SM. We show that a factor of two enhancement of the fermion couplings due to the higher representations implies a significant difference to the doublet case. Let us emphasize that in the case of the current model, all the fermion couplings to the Higgs boson, which is responsible for the fermion masses, increase. This is in contrast with, for instance, the MSSM, where couplings of up-type and down-type fermions change from the Standard Model differently, due to the fact that there are only doublets in the model. It is a common feature of higher Higgs representations that the doublet couplings are enhanced, which thus indicates that higher representations are involved.

We present a detailed Monte Carlo analysis of the central exclusive production of a triplet model Higgs boson for a number of parameter choices.

For  $c_H \leq 0.5$ , we have shown that a light  $H_1^0$  Higgs boson (of mass 120-150 GeV) can be observed with a  $4\sigma$  (or better) significance if a fixed rate trigger is used. We find that a fixed rate *single jet* trigger is optimal at low luminosities whereas a fixed rate *forward proton* trigger (i.e. one proton detected at 220m in conjunction with a central jet) is optimal at high luminosities.

The expected error in the Higgs mass measurement using forward proton detectors is small. For  $c_H = 0.2$ , we find that the mass of the Higgs boson is measured to better than 0.3 GeV, regardless of the luminosity/trigger scenarios. This is due to the excellent mass resolution of the forward detectors and the large number of events. For  $c_H = 0.5$ , there are less events and so the error in the mass measurement increases. However, regardless of the parameter choice, the mass measurement can always be made to better than 2 GeV if a fixed rate single jet trigger is used to retain events in which both protons are tagged at 420 m from the IP.

## Acknowledgments

We are grateful to Brian Cox, Albert De Roeck, Jeff Forshaw, John Gunion, Alan Martin, Risto Orava, Mark Owen, Misha Ryskin, Stefan Soldner-Rembold, and Marek Tasevsky for useful discussions. KH gratefully acknowledges support from the Academy of Finland (Project No. 115032). This work was funded in the UK by the STFC.

## References

- [1] H. Georgi and M. Machacek, Nucl. Phys. B **262** (1985) 463.
- [2] K. Huitu, J. Maalampi, A. Pietila and M. Raidal, Nucl. Phys. B **487**, 27 (1997); K. Huitu, P. N. Pandita and K. Puolamaki, Phys. Lett. B **415**, 156 (1997); K. Huitu, P. N. Pandita and K. Puolamaki, Phys. Lett. B **423**, 97 (1998); S. Chakrabarti, D. Choudhury, R. M. Godbole and B. Mukhopadhyaya, Phys. Lett. B **434**, 347 (1998); K. Huitu, P. N. Pandita and K. Puolamaki, arXiv:hep-ph/9904388. K. Huitu, J. Laitinen, J. Maalampi and N. Romanenko, Nucl. Phys. B **598** (2001) 13 [arXiv:hep-ph/0006261]; S. Godfrey, P. Kalyniak and N. Romanenko, Phys. Rev. D **65**, 033009 (2002); J. Maalampi and N. Romanenko, colliders,” Phys. Lett. B **532**, 202 (2002); S. Godfrey, P. Kalyniak and N. Romanenko, Phys. Lett. B **545**, 361 (2002); A. G. Akeroyd and M. Aoki, Phys. Rev. D **72**, 035011 (2005); B. Mukhopadhyaya and S. K. Rai, Phys. Lett. B **633**, 519 (2006); J. E. Cieza Montalvo, N. V. Cortez, J. Sa Borges and M. D. Tonasse, Nucl. Phys. B **756**, 1 (2006) [Erratum-ibid. B **796**, 422 (2008)]; T. Rommerskirchen and

- T. Hebbeker, J. Phys. G **33**, N47 (2007); T. Han, B. Mukhopadhyaya, Z. Si and K. Wang, Phys. Rev. D **76** (2007) 075013 [arXiv:0706.0441 [hep-ph]]; J. F. Gunion, C. Loomis and K. T. Pitts, Snowmass 96 [arXiv:hep-ph/9610237]; I. Dorsner and I. Mocioiu, Nucl. Phys. B **796** (2008) 123 [arXiv:0708.3332 [hep-ph]]; F. del Aguila and J. A. Aguilar-Saavedra, Nucl. Phys. B **813**, 22 (2009) [arXiv:0808.2468 [hep-ph]].
- [3] A. A. Johansen, N. G. Uraltsev and V. A. Khoze, Sov. J. Nucl. Phys. **46** (1987) 890 [Yad. Fiz. **46** (1987) 1502].
- [4] A. Kundu and B. Mukhopadhyaya, Int. J. Mod. Phys. A **11** (1996) 5221 [arXiv:hep-ph/9507305]; G. L. Kane, S. F. King and L. T. Wang, Phys. Rev. D **64** (2001) 095013 [arXiv:hep-ph/0010312]; C. P. Burgess, J. Matias and M. Pospelov, Int. J. Mod. Phys. A **17** (2002) 1841 [arXiv:hep-ph/9912459]; D. Choudhury, A. Datta and K. Huitu, Nucl. Phys. B **673** (2003) 385 [arXiv:hep-ph/0302141].
- [5] for a recent review see E. Accomando *et al.*, arXiv:hep-ph/0608079, see 'Higgs triplets' by John F. Gunion and Chris Hays, p. 497.
- [6] N. Arkani-Hamed, A. G. Cohen, E. Katz and A. E. Nelson, JHEP **0207** (2002) 034 [arXiv:hep-ph/0206021].
- [7] V.A. Khoze, A.D. Martin, M.G. Ryskin, Eur. Phys. J. C **23** (2002) 311 [arXiv:hep-ph/0111078].
- [8] M. G. Albrow *et al.* [FP420 R&D Collaboration], arXiv:0806.0302 [hep-ex].
- [9] J. J. van der Bij, Nucl. Phys. B **248** (1984) 141;
- [10] J. J. van der Bij, Nucl. Phys. B **267** (1986) 557.
- [11] M. B. Einhorn and J. Wudka, Phys. Rev. D **39**, 2758 (1989).
- [12] R. Barbieri, P. Ciafaloni and A. Strumia, Phys. Lett. B **317** (1993) 381.
- [13] V. Borodulin and G. Jikia, Phys. Lett. B **391** (1997) 434 [arXiv:hep-ph/9609447].
- [14] R. Akhoury, J. J. van der Bij and H. Wang, Eur. Phys. J. C **20** (2001) 497 [arXiv:hep-ph/0010187].
- [15] R. Boughezal, J. B. Tausk and J. J. van der Bij, Nucl. Phys. B **713** (2005) 278 [arXiv:hep-ph/0410216].
- [16] A. C. Longhitano, Phys. Rev. D **22** (1980) 1166.
- [17] J. van der Bij and M. J. G. Veltman, Nucl. Phys. B **231**, 205 (1984).

- [18] J. F. Gunion, H. E. Haber, G. L. Kane and S. Dawson, “The Higgs Hunter’s Guide,” Westview Press; J. F. Gunion, H. E. Haber, G. L. Kane and S. Dawson, arXiv:hep-ph/9302272.
- [19] J. Erler and P. Langacker, in W. M. Yao *et al.* [Particle Data Group], J. Phys. G **33** (2006) 1.
- [20] M. C. Chen, S. Dawson and C. B. Jackson, Phys. Rev. D **78** (2008) 093001 [arXiv:0809.4185 [hep-ph]].
- [21] M. S. Chanowitz and M. Golden, Phys. Lett. B **165** (1985) 105.
- [22] J. F. Gunion, R. Vega and J. Wudka, Phys. Rev. D **42** (1990) 1673.
- [23] J. F. Gunion, R. Vega and J. Wudka, Phys. Rev. D **43** (1991) 2322.
- [24] J. R. Ellis, M. K. Gaillard and D. V. Nanopoulos, Nucl. Phys. B **106**, 292 (1976); B. L. Ioffe and V. A. Khoze, Leningrad-76-274, November 1976, published in Sov. J. Part. Nucl. **9**, 50 (1978) [Fiz. Elem. Chast. Atom. Yadra **9**, 118 (1978)].
- [25] M. Aoki and S. Kanemura, Phys. Rev. D **77** (2008) 095009 [arXiv:0712.4053 [hep-ph]].
- [26] H. E. Haber and H. E. Logan, Phys. Rev. D **62** (2000) 015011 [arXiv:hep-ph/9909335]; K. Cheung and D. K. Ghosh, JHEP **0211** (2002) 048 [arXiv:hep-ph/0208254].
- [27] W. C. Yang [DO Collaboration], arXiv:0810.3219 [hep-ex];  
V. M. Abazov *et al.* [D0 Collaboration], Phys. Rev. Lett. **101** (2008) 071804 [arXiv:0805.2491 [hep-ex]].
- [28] A. De Roeck, V.A. Khoze, A.D. Martin, R. Orava and M.G. Ryskin, Eur. Phys. J. **C25** (2002) 391 [arXiv:hep-ph/0207042].
- [29] J. R. Forshaw, arXiv:0901.3037;  
J. Forshaw and A. Pilkington, In *\*Hamburg 2007, Blois07, Forward physics and QCD\* 130-136*.
- [30] P. J. Bussey, arXiv:0809.1335 [hep-ex];  
M. Grothe [CMS Collaboration], Nucl. Phys. Proc. Suppl. **179-180**, 173 (2008) [arXiv:0806.2977 [hep-ex]].
- [31] S. Heinemeyer *et al.* Eur. Phys. J. C **53**, 231 (2008) [arXiv:0708.3052 [hep-ph]];
- [32] S. Heinemeyer *et al.* arXiv:0811.4571 [hep-ph].

- [33] B. E. Cox, F. K. Loebinger and A. D. Pilkington, *JHEP* **0710** (2007) 090 [arXiv:0709.3035 [hep-ph]].
- [34] V.A. Khoze, A.D. Martin and M. Ryskin, *Eur. Phys. J. C* **19** (2001) 477 [Erratum-ibid. **C 20** (2001) 599], hep-ph/0011393.
- [35] A. Kaidalov, V.A. Khoze, A.D. Martin and M. Ryskin, *Eur. Phys. J. C* **33** (2004) 261, hep-ph/0311023.
- [36] J. R. Ellis, J. S. Lee and A. Pilaftsis, *Phys. Rev. D* **71**, 075007 (2005) [arXiv:hep-ph/0502251].
- [37] J. R. Forshaw, J. F. Gunion, L. Hodgkinson, A. Papaefstathiou and A. D. Pilkington, *JHEP* **0804**, 090 (2008) [arXiv:0712.3510 [hep-ph]].
- [38] V.A. Khoze, A.D. Martin, M.G. Ryskin, *Eur. Phys. J. C* **14** (2000) 525 [arXiv:hep-ph/0002072].
- [39] V.A. Khoze, A.D. Martin and M.G. Ryskin, *Eur. Phys. J. C* **18** (2000) 167 [arXiv:hep-ph/0007359].
- [40] M.G. Ryskin, A.D. Martin and V.A. Khoze, *Eur. Phys. J. C* **54**, 199 (2008); E.G.S. Luna *et al.*, arXiv:0807.4115 [hep-ph].
- [41] M. G. Ryskin, A. D. Martin and V. A. Khoze, arXiv:0812.2407 [hep-ph]; arXiv:0812.2413 [hep-ph].
- [42] V.A. Khoze, A.D. Martin and M.G. Ryskin, *Eur. Phys. J. C* **55** (2008) 363 [arXiv:0802.0177 [hep-ph]].
- [43] V. A. Khoze, A. D. Martin, M. G. Ryskin and W. J. Stirling, *Eur. Phys. J. C* **35** (2004) 211 [arXiv:hep-ph/0403218].
- [44] A. D. Martin, V. A. Khoze and M. G. Ryskin, arXiv:0810.3560 [hep-ph]; arXiv:0811.1481 [hep-ph].
- [45] V.A. Khoze, A.D. Martin and M.G. Ryskin, *JHEP* **0605** (2006) 036 [arXiv:hep-ph/0602247].
- [46] T. Aaltonen *et al.* [CDF Collaboration], *Phys. Rev. D* **77** (2008) 052004 [arXiv:0712.0604 [hep-ex]].
- [47] T. Aaltonen *et al.* [CDF Collaboration], *Phys. Rev. Lett.* **99**, 242002 (2007) [arXiv:0707.2374 [hep-ex]].
- [48] M. G. Albrow [CDF Collaboration], arXiv:0812.0612 [hep-ex].
- [49] A.B. Kaidalov, V.A. Khoze, A.D. Martin and M.G. Ryskin, *Eur. Phys. J. C* **21** (2001) 521 [arXiv:hep-ph/0105145].

- [50] J. Bartels, S. Bondarenko, K. Kutak and L. Motyka, Phys. Rev. D **73** (2006) 093004 [arXiv:hep-ph/0601128].
- [51] M. Albrow *et al.*, arXiv:0811.0120 [hep-ex].
- [52] P. J. Bussey and W. Plano, FPTrack (to be published).
- [53] J. Monk and A. Pilkington, Comput. Phys. Commun. **175**, 232 (2006) [arXiv:hep-ph/0502077].
- [54] J. Pumplin, D. R. Stump, J. Huston, H. L. Lai, P. Nadolsky and W. K. Tung, JHEP **0207** (2002) 012 [arXiv:hep-ph/0201195].
- [55] A. G. Shuvaev, V. A. Khoze, A. D. Martin and M. G. Ryskin, Eur. Phys. J. C **56** (2008) 467 [arXiv:0806.1447 [hep-ph]].
- [56] ATLAS: Detector and physics performance technical design report, Volume 1, pp 317-346, 1999. CERN-LHCC-99-14
- [57] V. A. Khoze, M. G. Ryskin and W. J. Stirling, Eur. Phys. J. C **48**, 477 (2006) [arXiv:hep-ph/0607134].
- [58] V. A. Khoze, A. D. Martin and M. G. Ryskin, Phys. Lett. B **650** (2007) 41 [arXiv:hep-ph/0702213].
- [59] G. Corcella *et al.*, arXiv:hep-ph/0210213.
- [60] J. M. Butterworth, J. R. Forshaw and M. H. Seymour, Z. Phys. C **72** (1996) 637 [arXiv:hep-ph/9601371].
- [61] C. M. Buttar *et al.*, “The underlying event”, HERA and the LHC proceedings part A, 2006. [hep-ph/0601013]
- [62] ATLAS: Detector and physics performance technical design report, Volume 1, pp 99-175, 1999. CERN-LHCC-99-14
- [63] P. J. Bussey, T. D. Coughlin, J. R. Forshaw and A. D. Pilkington, JHEP **0611**, 027 (2006) [arXiv:hep-ph/0607264].
- [64] V. A. Khoze, A. D. Martin and M. G. Ryskin, Eur. Phys. J. C **48**, 467 (2006) [arXiv:hep-ph/0605113].
- [65] M. Grothe *et al.*, CERN-CMS-NOTE-2006-54
- [66] CMS & TOTEM diffractive and forward physics working group, CERN/LHCC 2006-039/G-124, CMS Note 2007/002, TOTEM Note, December 2006.
- [67] S. N. White, arXiv:0707.1500 [hep-ex].

- [68] T. Han, B. Mukhopadhyaya, Z. Si and K. Wang, and Phys. Rev. D **76**, 075013 (2007) [arXiv:0706.0441 [hep-ph]].
- [69] N. Schul and K. Piotrkowski, at the Nucl. Phys. Proc. Suppl. **179-180**, 289 (2008) [arXiv:0806.1097 [hep-ph]].